Available online at www.sciencedirect.com
ScienceDirect
Journal of Molecular Catalysis A: Chemical 281 (2008) 93–98
JOURNAL OF MOLECULAR CATALYSIS A: CHEMICAL
www.elsevier.com/locate/molcata

MTBE visible-light photocatalytic decomposition over Au/TiO_2 and $Au/TiO_2–Al_2O_3$ sol–gel prepared catalysts

Vicente Rodríguez-González[a,b,*], Rodolfo Zanella[c], Gloria del Angel[a], Ricardo Gómez[a,**]

[a] *Universidad Autónoma Metropolitana-I, Depto. de Química, Av. San Rafael Atlixco No. 186, 09340 México, D.F., Mexico*
[b] *Instituto Mexicano del Petróleo, Dirección de Investigación y Postgrado/Eje Central 152, C.P. 07730 México, D.F., Mexico*
[c] *Centro de Ciencias Aplicadas y Desarrollo Tecnológico, UNAM, Circuito Exterior S/N, Ciudad Universitaria, Apartado Postal 70-186, Delegación Coyoacán, C.P. 04510, D.F., Mexico*

Available online 10 July 2007

Abstract

The synthesis, characterization and photoactivity for the MTBE decomposition on $Au/TiO_2–Al_2O_3$ and Au/TiO_2 sol–gel synthesized photocatalysts are reported. The semiconductor supports TiO_2, and $TiO_2–Al_2O_3$ were prepared by gelling titanium and aluminum alkoxides, whereas gold nanoparticles were prepared by the deposition–precipitation method with urea. Reference Au-supported photocatalysts were also prepared using the incipient impregnation method. Nitrogen adsorption as well as XRD, UV–vis and STEM-EDAX spectroscopies was used to characterize the solids. A shift of the band gap to the visible region was observed in gold-supported solids. The E_g band of the supports was shifted to the lower energy region for gold-supported catalysts. UV–vis characterization showed a gold plasmon surface resonance band (∼560 nm) in catalysts showing particles >7.0 nm. It is showed that the photocatalytic decomposition of MTBE in water (500 ppm) carried out with visible-light source (λ 495 nm) strongly depend of the Au particle size (6.4–25 nm). The catalysts with gold particle size ≤7.5 nm are the most active. It is proposed that in the catalyst with gold particle <7.0 nm the $Au^{\delta+}$ electrodeficiency is the responsible of the highest activity. Meanwhile, in catalysts with gold particles >7.0 nm the plasmon surface resonance band plays an important role in the photoactivity behavior.

Keywords: Doped titanium dioxide catalysts; MTBE photocatalytic decomposition; Gold–titania catalysts; Titania–alumina sol–gel catalysts; Gold titania–alumina catalysts

1. Introduction

The emerging field of nanostructured titania semiconductor [1–3] combined with gold-supported nanoparticles has acquired great interest in recent years for applications in the wastewater purification [4]. The presence of nanosized gold particles supported on titania shift the response of the photocatalysts into the visible region [5,6]. Great success has been reached in the preparation of gold nanoparticles over TiO_2 [7–9], however, the deposition of gold over modified titania was only slightly reported [10–14].

The study of gold deposited over modified titania for photocatalytic applications became an interesting topic to research. In this way the photocatalytic properties of TiO_2 can be improved in a synergistic effect and visible-light source can be used. With these in mind, we prepare alumina–titania mixed oxides by the sol–gel method using aluminum and titanium alkoxides as precursors. Alumina was chosen because it can improve the textural properties of TiO_2 (e.g. high specific surface area) and dope in some extend the titania bulk. The deposition–precipitation method with urea was used for the impregnation of gold, since it has been reported that with this method highly dispersed gold particles were obtained [15]. The characterization of the solids was made by means of nitrogen adsorption, XRD, UV–vis and STEM-EDAX spectroscopies. The photocatalytic properties were evaluated in the liquid phase decomposition of methyl ter-butyl ether (MTBE) which is a well-known toxic wastewater pollutant. On the best of our knowledge only few researches has been previously reported for the decomposition of MTBE using TiO_2 [16–19] or Au-supported on titanium dioxide [20] and no one has been reported for the photo-decomposition of MTBE using gold-supported over titania–alumina mixed oxide.

* Corresponding author at: Universidad Autónoma Metropolitana-I, Depto. de Química, Av. San Rafael Atlixco No. 186, 09340 México, D.F., Mexico.
** Corresponding author. Tel.: +52 5558044668; fax: +52 5558044666.
E-mail addresses: vrg@xanum.uam.mx (V. Rodríguez-González), gomr@xanum.uam.mx (R. Gómez).

1381-1169/$ – see front matter © 2007 Published by Elsevier B.V.
doi:10.1016/j.molcata.2007.07.009

2. Experimental

2.1. Preparation of titania–alumina mixed oxide

The sol–gel titania and titania–alumina oxides were prepared as follows: 14 mL of aluminum ter-butoxide (Aldrich 98%) and 63 mL of titanium sec-butoxide (Aldrich 98%) were simultaneously added to a solution containing 115 mL of distilled water and 189 mL of *n*-butanol (Baker 99%). Then, the gelling solution was refluxed at 70 °C under constant stirring. The quantities of aluminum ter-butoxide and titanium sec-butoxide were calculated to provide 10 wt% loading of alumina in the final mixed oxide. Additionally, a bare TiO_2 sol–gel catalyst was prepared in analogous way. The formation of the gel was obtained with controlled hydrolysis–condensation reactions at 70 °C during 48 h at pH 7. Afterwards, the samples were evaporated in a rotavapor at 80 °C and then dried in an oven for 12 h at 80 °C. Finally, the excess of the solvent and water was removed by annealing the materials in air at 500 °C for 4 h with a heating program rate of 2 °C/min. Additionally, commercial TiO_2 P25 from Degussa was thermally treated in an identical way to that used for the TiO_2 and TiO_2–Al_2O_3 sol–gel prepared semiconductors.

2.2. Gold deposition

Before the gold deposition, the supports were dried in air at 100 °C for 24 h. The preparations were made in the absence of light, since it is known that light decomposes and reduce gold precursors. The preparation of gold nanoparticles was performed by deposition–precipitation with urea (DP urea) [8,15] as follows: 1 g of the support was added to 60 mL of an aqueous solution containing $HAuCl_4$ (Aldrich 99.9 %) (4.2×10^{-3} M) and urea (Aldrich 99%) (0.42 M). The initial pH value was ~2. Then, the suspension was heated at 80 °C and vigorously stirred for 16 h. Urea decomposition leads to a gradual rise in pH from 2 to 7. The amount of gold in the solution corresponds to a gold loading of 1 wt% on the support, Table 1. Once made the gold deposition the catalysts were reduced in hydrogen flow (100 ml/min) at 200 °C for 4 h [21].

For comparative purposes Au/P25 catalyst was prepared by deposition–precipitation with urea in the same way used for the Au/TiO_2 and Au/TiO_2–Al_2O_3 sol–gel supports. Additionally, two samples were prepared by incipient impregnation with $HAuCl_4$. The impregnated sample was kept at room temperature for 2 h, dried under vacuum at 100 °C for 2 h and then thermally treated in hydrogen with a flow rate of 100 ml/min at 200 °C for 4 h. The obtained samples were labeled as Au-imp/P25 and Au-imp/TiO_2–Al_2O_3.

Table 1
Textural and photophysical characterization of supports and gold-supported photocatalysts

Material	S BET ($m^2\ g^{-1}$)	Pore size (nm)	E_g (eV)	λ_1 (nm)
P25	54	–	3.10	399
TiO_2	65	13	3.13	395
TiO_2–Al_2O_3	237	13	3.23	384
Au/P25	56	56	2.68	459
Au/TiO_2	66	11	2.74	450
Au/TiO_2–Al_2O_3	241	10	3.10	394
Au-imp/P25	48	–	3.00	420
Au-imp/TiO_2–Al_2O_3	220	9	3.12	380

2.3. Characterization

The specific surface area of the semiconductors and gold-supported photocatalysts were determined by N_2 adsorption in a Quantachrome sorptometer apparatus. Specific surface areas (BET) and pore size distribution (BJH) were calculated from the nitrogen adsorption–desorption isotherms. The crystalline phase was determined by X-ray diffraction (XRD) with a Bruker D-8 Diffractometer using Cu Kα radiation at a step of 0.03 of 2θ. Transmission electron microscopy (TEM) and EDAX studies were made with a Tecnai T20, 200 kV TEM/Nano-Analysis system with 0.4 nm as resolution. Gold mean particle size was calculated using the DigitalMicrograph (TM) 3.7.0 for GMS 1.2 by the Gatan Software Team coupled to the STEM computer. UV–visible spectra (200–900 nm) of the materials were obtained with an UV–vis spectrophotometer Varian Cary 100 (diffuse reflectance). The band gap of the solids was calculated by linearization of the slope to the *X*-axis for *Y*-axis equal 0 [22].

2.4. Evaluation of the photocatalytic activity in the MTBE photo-decomposition

The photocatalytic activities of supports and gold-supported photocatalysts were evaluated in the degradation of MTBE (Aldrich 99%) 500 ppm in water (200 mL) under visible irradiation. A visible krypton lamp (90-0014-01, λ 495 nm) standard Pen-Ray lamp from UVP Corporation was used for irradiation. The lamp was protected with a quartz tube and immersed in the solution. The photoreaction was carried out in a slurry Pyrex sealed reactor (250 mL) under constant magnetic stirring in the presence of 100 mg of catalyst. Before the activity test, dry air (1 mL/s) was bubbled for 30 min in the dark in order to reach the dissolved oxygen saturation and MTBE adsorption. The progress of the photo-chemical decomposition was monitored by measuring at various interval of time the total organic carbon (TOC analyzer model TOC-5000, Shimadzu Seisakusho Co., Tokyo, Japan). The identification of the by-products was made by Gas chromatography–mass spectrometry (GC/MS) analysis using a HP GC–MS model 5973 (Column: 50M. PONA Crosslinked Methyl Siloxane 0.2 mm × 0.5 μm film, HP).

3. Results

The nitrogen adsorption/desorption isotherms of the sol–gel supports and Au-deposited by deposition–precipitation with urea are shown in Fig. 1. A remarkable difference can be observed between the titania–alumina oxide and bare TiO_2 catalysts. All the isotherms present hysteresis loop and they can be classified as Type IV mesoporous materials. The specific surface area for titania–alumina support was 237 m^2/g, meanwhile for bare TiO_2 and P25 from Degussa the BET specific surface areas

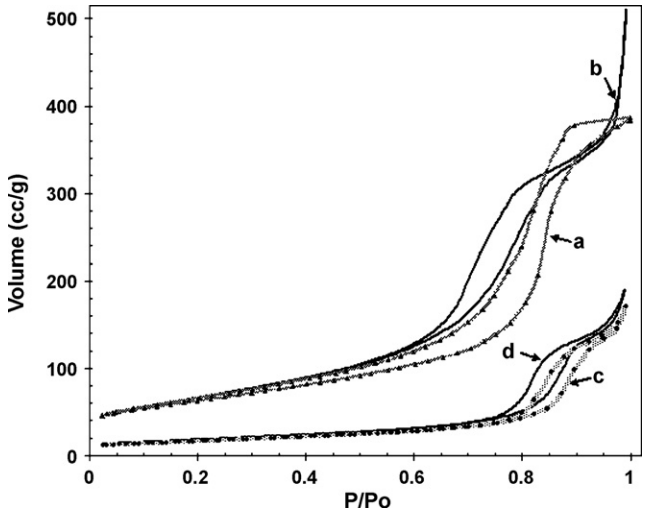

Fig. 1. Adsorption–desorption nitrogen isotherms of supports and gold-supported photocatalysts: (a) TiO_2–Al_2O_3; (b) Au/TiO_2–Al_2O_3; (c) bare TiO_2 sol–gel; (d) Au/TiO_2 sol–gel.

were 54 and 65 m^2/g, respectively. The co-gelling of titanium and aluminum alkoxides produce solids with specific surface area four times higher than that obtained in the bare sol–gel titania (Table 1). Note that on gold-supported catalysts the specific surface areas and the mean pores size diameter are practically of the same order of supports.

XRD spectra of selected samples are shown in Fig. 2. The diffraction patterns of the sol–gel prepared catalysts annealed at 500 °C only show anatase as the crystalline phase. For titania P25 the well established presence of anatase and rutile phases can be seen. The presence of gold is not detected in any diffractrogram suggesting the formation of nanosized gold particles.

Selected STEM images for the gold-supported photocatalysts are shown in Figs. 3–5. The STEM images denote the presence of gold-nanosized particles. The mean diameters calculated after counting around 80–100 particles were: 6.4, 7.5 and 11.0 nm for Au/TiO_2–Al_2O_3, Au/P25 and Au/TiO_2, respectively. On the other hand, for incipient impregnated preparations

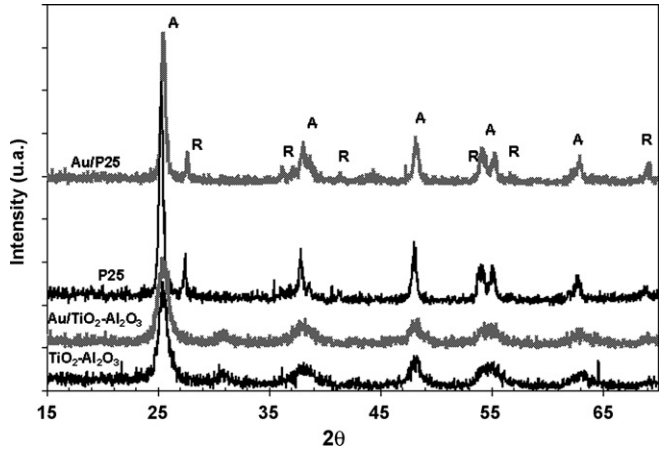

Fig. 2. XRD of commercial TiO_2-P25, mixed oxide TiO_2–Al_2O_3, Au/P25 and Au/TiO_2–Al_2O_3 semiconductor catalysts.

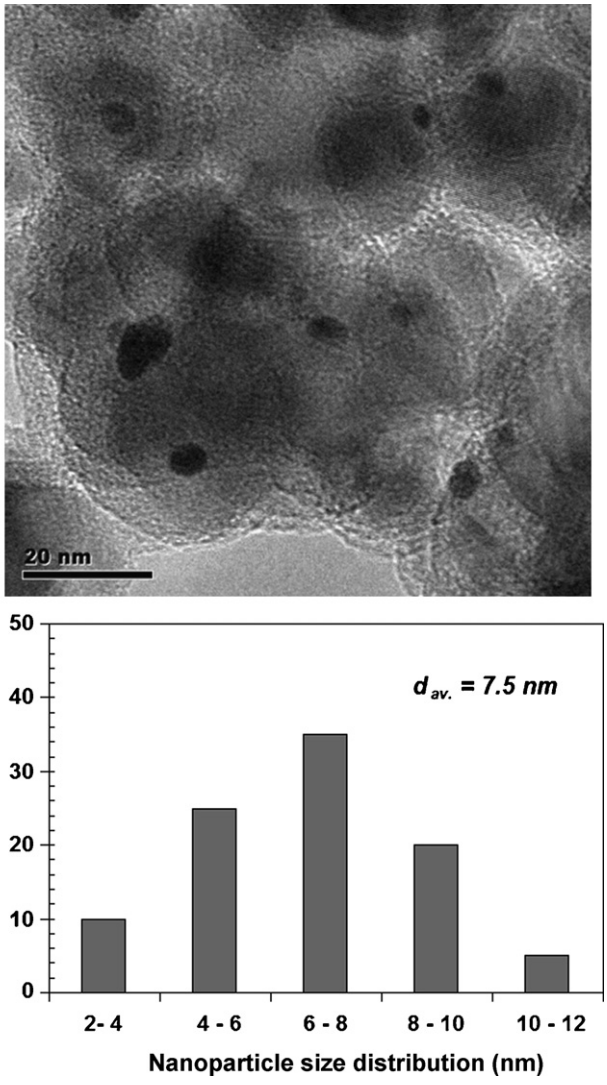

Fig. 3. TEM image of Au/P25 photocatalyst.

the particle size values were increased (20 and 25 nm for Au-imp/TiO_2–Al_2O_3 and Au-imp/P25, respectively). These results showed that the deposition–precipitation method allows the highest gold dispersion.

EDAX analysis showed gold and Ti values close to that of the nominal composition of the gold-supported catalysts Fig. 6a and b.

The diffuse adsorption spectra of the gold-supported photocatalysts are shown in Fig. 7. The TiO_2 band gap appears in the 380–459 nm region. Additionally ca. 560 nm a broad absorption band assigned to the gold plasmon surface resonance band is observed for Au/TiO_2 and Au/P25 catalysts as well as for Au-imp/TiO_2–Al_2O_3 and Au-imp/P25 impregnated catalysts. For the Au/TiO_2–Al_2O_3 catalyst a very bad resolved plasmon surface resonance adsorption band in the visible region is observed. The gold plasmon resonance band was associated to gold particles with a diameter higher than 5 nm [6]. Kamat [6] reports that the surface plasmon resonance of metallic nanoparticles is sensitive to the particle size, load and surrounding environment.

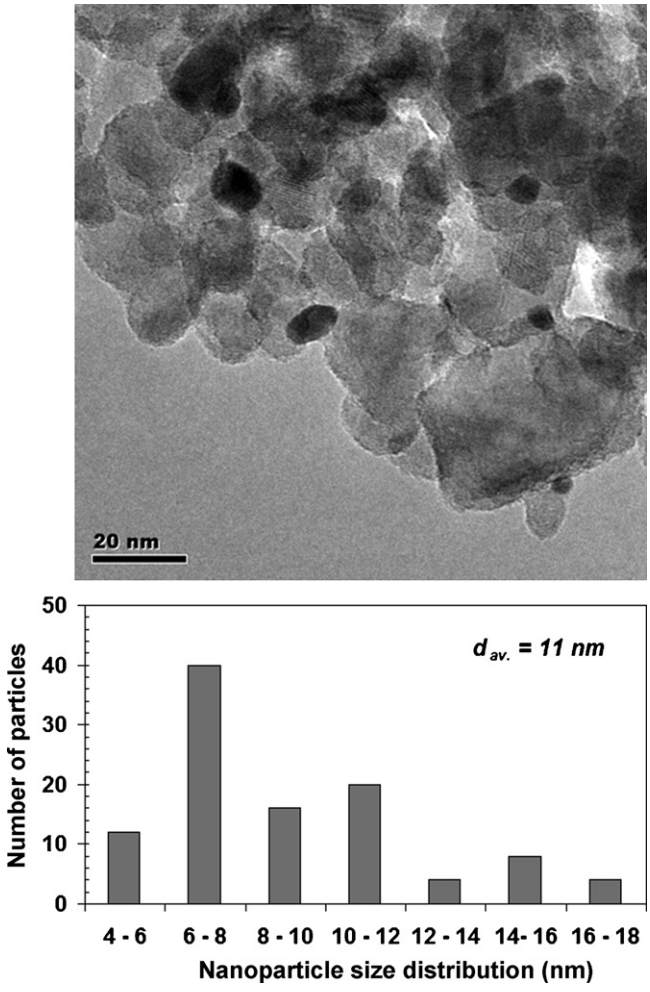

Fig. 4. TEM image of Au/TiO_2 sol–gel photocatalyst.

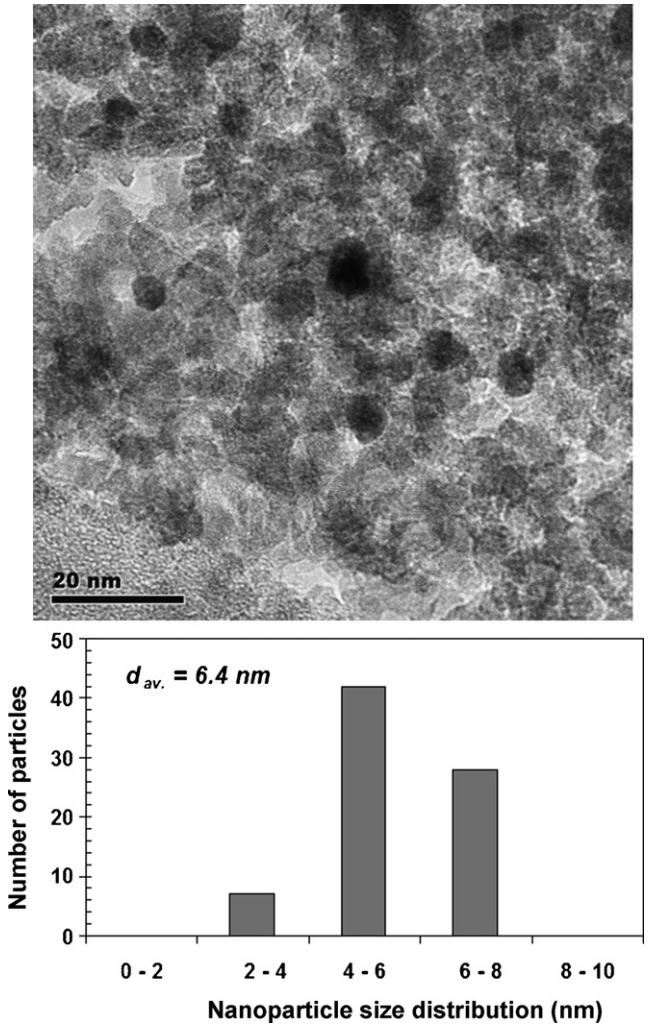

Fig. 5. TEM image of $Au/TiO_2–Al_2O_3$ sol–gel photocatalyst.

The MTBE photodegradation kinetics was expressed as TOC (total organic carbon) as a function of time. In Fig. 8 the dark adsorption of MTBE is illustrated for the $Au/TiO_2–Al_2O_3$ catalyst and $TiO_2–Al_2O_3$ support. It represents around 7–10% of the initial MTBE concentration and it reaches the equilibrium after a contact time of 30 min. The photolysis and visible-light MTBE photodegradation was also illustrated in Fig. 8. Since dark adsorption is not negligible (ca. 10%) in supports and catalysts, the evolution of the MTBE photodegradation in gold-supported catalysts was evaluated after 30 min in dark. The normalized TOC/TOC_0 as a function of the time for the various gold-supported catalysts is shown in Fig. 9 were gold impregnated catalysts showed very low activity. The MTBE converted after 150 min in photodegradation was 20% and 27% for Au-imp/P25 and Au-imp/$TiO_2–Al_2O_3$ catalysts, respectively; these results which contrast with the highest photoactivity showed by the gold deposition–precipitation preparations. The MTBE photodegradation for these catalysts were 57%, 80% and 100% for Au/TiO_2, Au/P25, and $Au/TiO_2–Al_2O_3$ photocatalysts, respectively. The MTBE photodegradation was total on the $Au/TiO_2–Al_2O_3$ catalyst. To explain this behavior it is interesting to analyze the following points: (i) the E_g values of the supports was shifted to lower energy region in Au-supported catalysts (Table 1); (ii) the specific surface area of the solids can be ruled out as important factor, since on $Au/TiO_2–Al_2O_3$ and Au-imp/$TiO_2–Al_2O_3$ catalysts the BET areas are of the same order (240 and 220 m^2/g, respectively) and the activity is quite different; (iii) all the photocatalysts showed plasmon surface resonance with exception of the most active of them, the $Au/TiO_2–Al_2O_3$ catalyst.

We mentioned before that the plasmon surface resonance is related to the particles size, in our case it can be seen in the visible region for catalysts showing gold particles larger than 7.0 nm. In fact we have catalysts with a large range in gold particle size (6.4–25 nm) so it is possible to correlate the particle size to the photoactivity. The TOC obtained after 150 min in photodegradation as a function of the particle size is presented in Fig. 10. The figure shows that the MTBE conversion strongly depends on the particle size. The small particles are the most active. A high activity for small Au particles has also been observed by Orlov et al. [20,23] in MTBE and 4-cholophenol photodegradation over Au/TiO_2 supported catalysts (Table 2). A critical gold particle size <5 nm for a maximum in activity was reported. Similar behavior of gold-nanosized particles in the oxidation of CO has also been reported by Haruta [24] who shows that gold particles smaller than 5 nm are the most active.

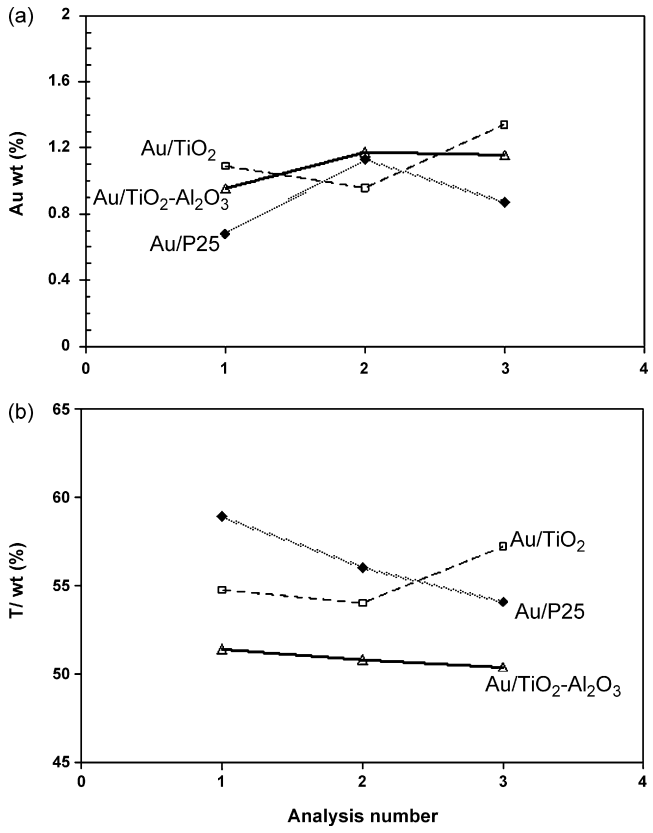

Fig. 6. EDAX analysis for sol–gel Au-supported photocatalysts (a) gold wt% and (b) titanium wt%.

The dependence of the activity in function of the particle size has also been observed for a large kind of supported metals in heterogeneous gas phase reactions. For example, it has been reported on Pd/Al_2O_3 [25] and Rh/Al_2O_3 [26,27] that small particles showed the highest activity in hydrocarbons hydrogenation reactions. The explanation of such high activity is given in function of the electron deficiency which showed particles smaller than 2.0 nm. For palladium the $Pd^{\delta+}$ species, determined by various techniques and methods, is reported as the responsible of the increasing activity [28].

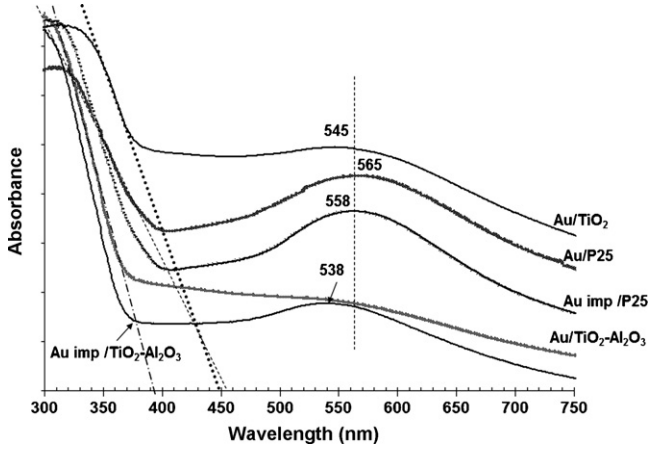

Fig. 7. Diffuse absorbance spectra of gold photocatalysts.

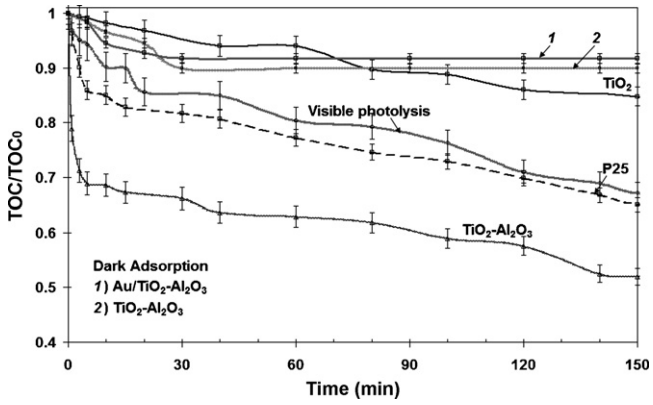

Fig. 8. MTBE photo-decomposition as a function of the time under visible irradiation on titania supports.

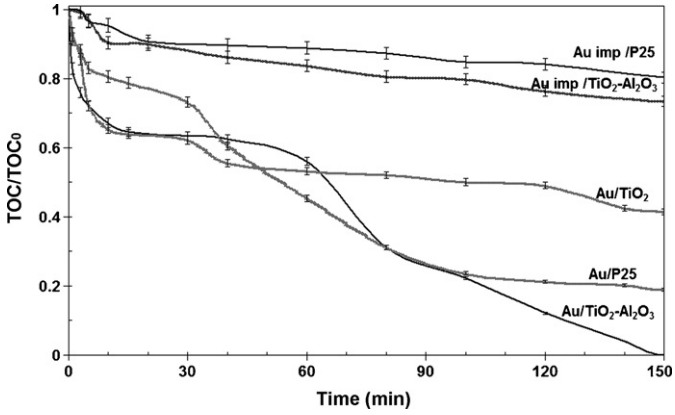

Fig. 9. MTBE photo-decomposition as a function of time under visible irradiation on gold photocatalsyts.

Gold particles on TiO_2, TiO_2–Al_2O_3 and P25 prepared by the deposition–precipitation methods are nanosized particles and they cannot be resolved in the XRD spectra [29]. Jakob et al. [30] report that the excited electrons are transferred from TiO_2 to Au nanoparticles, improving the charge separation in semiconductor/metal photocatalysts and hence the photocatalytic reactivity. The smaller the particle size the bigger will be the gold electron deficiency as discussed above for noble metals.

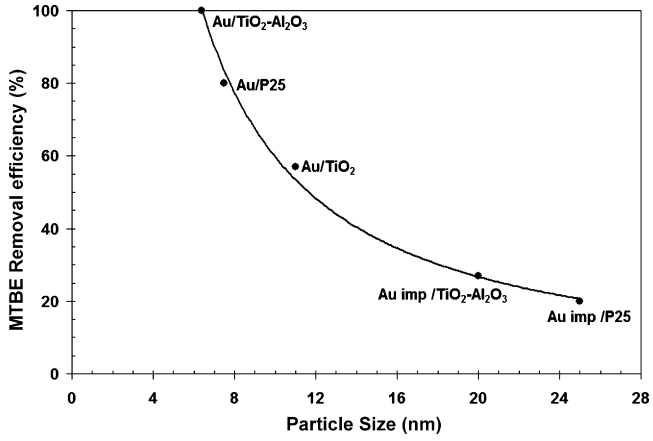

Fig. 10. MTBE removal efficiency as a function of the gold particle size.

Table 2
MTBE conversion, gold particle size calculated from TEM and plasmon surface resonance absorption band in gold-supported photocatalysts

Photocatalyst	% TOC/TOCo	Particle size (nm)	Plasmon resonance absorption
Au/P25	80	7.5	565
Au/TiO_2	57	11.0	545
Au/TiO_2–Al_2O_3	100	6.4	–
Au-imp/P25	20	25.0	558
Au-imp/TiO_2–Al_2O_3	27	20.0	538

A great number of variables can play simultaneously important roles in the MTBE photodegradation. However, in our catalytic systems the big difference is around the plasmon surface resonance band presented by the gold-supported catalysts in the visible region and of course in the particle size showed for the various photocatalysts.

Firstly, in small particles (<7.0 nm) we assume the formation of $Au^{\delta+}$ species. After light-excitation the recombination rate of the electron-hole pair was diminished and the importance on the recombination rate will depend of the charge deficiency in the gold nanoparticles. The maximum in photoactivity will correspond to small particles <7.0 nm, as it has been observed by Orlov et al. [20,23]. In such case a deep MTBE photodegradation occurs by the traditional oxidation photochemical mechanism in which titania holes generated the oxidation of the organic compounds.

On the other hand when the particle size is >7.0 nm the Au electrodeficiency diminishes. The recombination rate of the electron-hole pair is then less affected. In these catalysts the gold plasmon surface resonance plays an important role in the MTBE degradation pathway. The dipole effect formed in the gold plasmon stabilize the by-products *iso*-butyl alcohol, terbutyl alcohol, and formaldehyde, identified by MS–GC, which are organic molecules with major difficult to be photodecomposed. In such case the total photo-decomposition of MTBE is not reached and important amount of organic by-products remains in the photodegraded solution.

4. Conclusions

The main conclusions of the present work are the following: (i) gold nanoparticles (6.4–11 nm) can be prepared by deposition–precipitation with urea over TiO_2 and TiO_2–Al_2O_3 sol–gel supports as well as P25 commercial titania; (ii) in gold-supported catalysts prepared by incipient impregnation large particles (20–25 nm) were formed; (iii) a shift on the band gap energy of the supports to the visible region is observed in gold-supported photocatalysts; (iv) in the MTBE photodegradation with visible-light source the gold particles smaller than 7.0 nm are the most active; (v) a dependence in photoactivity and gold particle size was observed in the MTBE photocatalytic degradation; (vi) in particles larger than 7.0 nm gold plasmon surface resonance band is observed in the visible region.

Acknowledgements

We would like to gratefully acknowledge the STEM support given by F.M. Moran-Pineda (IMP), and the technical assistance of G. Mendoza and C. Guzman. R. Zanella is indebted to UNAM Nanoscience and Nanotechnology project DGAPA IN106507 grant.

References

[1] A. Fujishima, T.N. Rao, D.A. Tryk, J. Photochem. Photobial C: Photochem. Rev. 1 (2000) 1–21.
[2] O.M. Alfano, D. Bahnemann, A.E. Cassano, R. Dillert, R. Goslich, Catal. Today 58 (2000) 199.
[3] U. Diebold, Surf. Sci. Rep. 48 (2003) 53–229.
[4] K. Hashimoto, H. Irie, A. Fujishima, Jpn. J. Appl. Phys. 44 (2005) 8269.
[5] S. Zhao, S. Chen, S. Wang, Z. Quan, J. Colloid Interface Sci. 221 (2000) 161.
[6] P.V. Kamat, J. Phys. Chem. B 106 (2002) 7729.
[7] M. Haruta, CATTECH 6 (2002) 102.
[8] R. Zanella, L. Delannoy, C. Louis, Appl. Catal. A: Gen. 291 (2005) 62.
[9] B. Schumacher, V. Plzak, J. Cai, R.J. Behm, Catal. Lett. 101 (2005) 215.
[10] M. Jung, J. Sol–Gel Sci. Technol. 19 (2000) 563–568.
[11] M.A. Debeila, R.P.K. Wells, J.A. Anderson, J. Catal. 239 (2006) 162.
[12] M.A. Centeno, M. Paulis, M. Montes, J.A. Odriozola, Appl. Catal. B: Environ. 61 (2005) 177.
[13] A.G. Agrios, P. Pichat, J. Appl. Electrochem. 35 (2005) 655–663.
[14] R.S. Sonawane, M.K. Dongare, J. Mol. Catal. A: Chem. 243 (2006) 68.
[15] R. Zanella, S. Giorgio, C.R. Henry, C. Louis, J. Phys. Chem. B 106 (2002) 7634.
[16] R.D. Barreto, K.A. Gray, K. Anders, Water Res. 29 (1995) 1243.
[17] E. Sahle-Demessie, J. Enriquez, G. Gupta, Water Environ. Res. 74 (2002) 122.
[18] S.E. Park, H. Joo, J.W. Kang, Solar Energy Mater. Solar Cells 80 (2003) 73.
[19] Y. Zang, R. Farnood, Appl. Catal. B: Environ. 57 (2005) 275.
[20] A. Orlov, D.A. Jefferson, M. Tikhov, R.M. Lambert, Catal. Commun. 8 (2007) 821.
[21] R. Zanella, C. Louis, Catal. Today 768 (2005) 107.
[22] R. Gomez, T. Lopez, E. Ortiz-Islas, J. Navarrete, E. Sanchez, F. Tzompantzi, X. Bokhimi, J. Mol. Catal. A: Chem. 193 (2003) 217.
[23] A. Orlov, D.A. Jefferson, N. Macleod, R.M. Lambert, Catal. Lett. 92 (2004) 41.
[24] M. Haruta, Catal. Today 36 (1997) 153.
[25] R. Gómez, O. Novaro, Rect. Kinet. Catal. Lett. 45 (1991) 251.
[26] S. Fuentes, F. Figueras, R. Gómez, J. Catal. 68 (1981) 419.
[27] G. Del Angel, B. Coq, F. Figueras, S. Fuentes, R. Gómez, Nouveau J. Chim. 9 (1983) 173.
[28] F. Figueras, R. Gómez, M. Primet, in: W.M. Meir, J.B. Uytterhoeven (Eds.), Advances in Chemistry Series, 121, 1973, p. 480.
[29] C. Meneghini, S. Mobilio, F. Pivetti, I. Selmi, M. Prudenziati, B. Morten, J. Appl. Phys. 86 (1999) 3590.
[30] M. Jacob, H. Levanon, P.V. Kamat, Nano Lett. 3 (2003) 353.